Research Article

Thermal instability of an Oldroyd-B fluid-saturated porous layer: implications of pressure gradient and LTNE temperatures

C. Hemanthkumar[1] · I. S. Shivakumara[1]

Received: 17 January 2020 / Accepted: 28 February 2020 / Published online: 6 March 2020

Abstract
A local thermal nonequilibrium model is used to investigate the instability of an Oldroyd-B fluid-saturated horizontal layer of porous medium by imposing a constant pressure gradient in the horizontal direction and maintaining a constant temperature difference between the boundaries. The flow in the porous medium is studied by a modified Darcy–Oldroyd-B model. The problem has been transformed into a generalized complex eigenvalue problem and solved numerically by utilizing the Galerkin method. The pressure gradient and/or the viscoelasticity of the fluid instill oscillatory instability. The influence of constant horizontal pressure gradient is to hasten the onset of oscillatory convection: a result of contrast noticed in Newtonian fluids. The impact of constant horizontal pressure gradient is to increase the critical frequency of oscillations and to increase the size of convection cells. Besides, the effect of viscoelastic parameters on the oscillatory onset diminishes in the presence of pressure gradient. For the Maxwell fluid, instability sets in earlier compared to an Oldroyd-B fluid. The numerical results obtained under the limiting case are shown to be in excellent agreement with the published ones.

Keywords Horizontal pressure gradient · Oldroyd-B fluid · Porous layer · Local thermal nonequilibrium · Oscillatory convection · Galerkin approach

List of symbols

a	Wave number in the x-direction
c	Specific heat
d	Depth of the porous layer
$D = \mathrm{d}/\mathrm{d}z$	Differential operator
$\mathbf{g}$	Acceleration due to gravity
h	Interphase heat transfer coefficient
H	Scaled interphase heat transfer coefficient ($H = hd^2/\varepsilon k_\mathrm{f}$)
k	Thermal conductivity
K	Permeability
p	Pressure
P	Modified pressure
$\mathbf{q}$	Velocity vector
R_D	Darcy–Rayleigh number ($R_\mathrm{D} = \rho_0 g\beta\Delta TKd(\rho c)_\mathrm{f}/\varepsilon\mu_\mathrm{f}k_\mathrm{f}$)
t	Time
T	Temperature
W	Amplitude of perturbed vertical velocity
(x, y, z)	Cartesian coordinates

Greek symbol

α	Ratio of thermal diffusivities ($\alpha = \kappa_\mathrm{f}/\kappa_\mathrm{s}$)
γ	Porosity-modified conductivities ratio ($\gamma = \varepsilon k_\mathrm{f}/(1-\varepsilon)k_\mathrm{s}$)
β	Coefficient of thermal expansion of the fluid
ε	Porosity
λ_1	Stress relaxation time
λ_2	Strain retardation time
Λ_1	Stress relaxation parameter ($\Lambda_1 = \lambda_1 k_\mathrm{f}/(\rho c)_\mathrm{f} d^2$)
Λ_2	Strain retardation parameter ($\Lambda_2 = \lambda_2 k_\mathrm{f}/(\rho c)_\mathrm{f} d^2$)
μ_f	Dynamic viscosity of the fluid
ρ	Fluid density

✉ C. Hemanthkumar, c.hemanthkumar6@gmail.com | [1]Department of Mathematics, Bangalore University, Bengaluru 560 056, India.

ρ_0	Fluid density at $T = T_0$
Π	Horizontal pressure gradient
ϕ	Solid temperature
Φ	Amplitude of solid temperature
θ	Fluid temperature
Θ	Amplitude of fluid temperature
ψ	Stream function
Ψ	Amplitude of stream function
ω	Growth factor

Subscripts

b	Basic state
c	Critical value
f	Fluid phase
s	Solid phase

Superscripts

*	Dimensionless quantity
′	Perturbed quantity

1 Introduction

In the study of thermal convection in a porous medium, the elemental volume-averaged temperatures of the fluid phase and the solid phase are identical or different and heat transfer between them is a matter of concern and it depends on the situation in hand. The former contemplation is called the local thermal equilibrium (LTE) model, and the latter is called the local thermal nonequilibrium (LTNE) model. It is experimentally observed that the LTE model requires numerous constraints and this assumption is no longer valid when the particles or pores are not small enough, when the thermal properties differ widely, or when the convective transport is important [1–3]. These restrictions enforced the inevitability of switching over to LTNE model in the study of thermal convection in porous media.

Thermogravitational convection in fluid-saturated porous media using a LTNE model has been studied extensively due to its applications in various fields of science and engineering, for example, building thermal insulation, nuclear reactor maintenance, nuclear waste disposal, oil reservoir, geothermal energy utilization and porous insert for thermal enhancement, to mention a few (Virto et al. [4]). In a detailed manner, Banu and Rees [5] studied buoyancy-driven convection in a layer of Darcy porous medium. Subsequently, many researchers extended this study under various additional effects [6–13]. An exhaustive bibliography on this topic can be found in the review article by Rees and Pop [14] and in the book by Neild and Bejan [15].

The study of non-Newtonian fluids in a porous medium is of prime significance in numerous fields such as petroleum, nuclear and chemical industries, reservoir engineering and bioengineering. The heavy crude is non-Newtonian and the rheology of such fluids depends on a generalized Darcy equation, which considers non-Newtonian behavior of fluids. Specifically, some oil sand contains waxy crude at shallow depth in the reservoir which is viewed as a viscoelastic fluid. Generalized Darcy equation is beneficial to the investigation of portability control in the displacement of oil mechanism, which increases the productivity of the oil recuperation. The onset of convection in a viscoelastic fluid-saturated porous layer has been studied extensively using a LTE model, and little consideration has been given toward the study using a LTNE model. Thermal convective instability of an Oldroyd-B fluid-saturated porous layer using a LTNE model was investigated by Malashetty et al. [16] and Shivakumara et al. [17]. The convective instability of Maxwell fluid-saturated porous layer using a LTNE model was studied by Malashetty and Kulkarni [18]. Recently, Shankar and Shivakumara [19] investigated the effect of LTNE on the stability of natural convection in an Oldroyd-B fluid-saturated vertical porous layer. All these studies confirmed that the oscillatory convection is the preferred mode of instability.

Copious literature is available on mixed (forced and free) convective flow in a porous medium. However, the studies on the impact of applied pressure gradient on buoyancy-driven convection in a fluid-saturated porous layer are still in infancy. These studies are found to be more relevant to model realistic effects occurring in several applications such as heat exchanger, sink simulation and cooling/heating design of the system, to mention a few. The influence of horizontal fluid motion on thermally induced convection currents in a layer of porous medium was investigated by Prats [20] using a LTE model. He showed that the basic flow and convection pattern move with the same speed in the same direction. The effect of inertia on the onset of mixed convection in a porous medium using a LTNE model was considered by Postelnicu [21]. Later, Postelnicu [22] studied the effect of a constant horizontal pressure gradient on the onset of Darcy–Bénard convection in a Newtonian fluid-saturated porous layer with LTNE model.

The existing studies on the onset of mixed convection are limited to Newtonian fluids-saturated porous media. Nonetheless, the consideration of non-Newtonian fluids is warranted in many applications such as ceramic processing, enhanced oil recovery, filtration and liquid composite molding. The intent of the current study is to examine the effect of a constant horizontal pressure gradient and viscoelasticity of the fluid on the onset of thermal convection in a fluid-saturated porous medium using a LTNE model. A modified Darcy–Oldroyd-B formulation is adopted to analyze the flow in the porous medium. The presence of constant pressure gradient affects the basic velocity, and also the stability

equations involve complex coefficients. The stability eigenvalue problem is numerically solved using the Galerkin method, and the results are tabulated and exhibited graphically for different values of governing parameters. Attempts are also made to obtain the solution analytically for the onset of convection using a single-term Galerkin expansion technique. The results obtained from the single-term Galerkin method are found to be in close agreement with those computed from the higher order Galerkin method.

2 Mathematical formulation

The schematic representation consists of an incompressible Oldroyd-B fluid-saturated porous layer bounded by the horizontal surfaces $z = 0$ and $z = d$(see Fig. 1), and these surfaces are held at fixed temperatures T_l and $T_u(< T_l)$, respectively. The x-axis is taken along the horizontal direction, and the gravity acts vertically downward. In the horizontal direction, a constant pressure gradient is applied. The fluid and solid phases of the porous medium possess different temperatures as the LTNE model is invoked.

The governing equations under the Oberbeck–Boussinesq approximation are [16, 17, 19]:

$$\nabla \cdot \mathbf{q} = 0, \tag{1}$$

$$\left(1 + \lambda_1 \frac{\partial}{\partial t}\right)\left(-\rho_f \mathbf{g} + \nabla p\right) = -\frac{\mu_\mathrm{f}}{K}\left(1 + \lambda_2 \frac{\partial}{\partial t}\right)\mathbf{q}, \tag{2}$$

$$(\rho c)_\mathrm{f}\left(\varepsilon \frac{\partial T_\mathrm{f}}{\partial t} + (\mathbf{q}.\nabla)T_\mathrm{f}\right) = \varepsilon k_\mathrm{f} \nabla^2 T_\mathrm{f} - (T_\mathrm{f} - T_\mathrm{s})h, \tag{3}$$

$$(\rho c)_\mathrm{s}(1-\varepsilon)\frac{\partial Ts}{\partial t} = k_\mathrm{s}(1-\varepsilon)\nabla^2 T_\mathrm{s} + (T_\mathrm{f} - T_\mathrm{s})h, \tag{4}$$

$$\rho_f = \rho_0[1 - \beta(T_\mathrm{f} - T_\mathrm{u})], \tag{5}$$

where $\mathbf{q} = (u, 0, w)$ is the velocity vector, p is the pressure, ρ_f is the density of the fluid, $\mathbf{g}$ is the gravitational acceleration, μ is the fluid viscosity, λ_1 and λ_2 are the stress relaxation and strain retardation time constants, K is the permeability, ε is the porosity, T_f and T_s are, respectively, the temperature of fluid and solid phases,h is the interphase heat transfer coefficient, β is the thermal expansion coefficient, c is the specific heat, $\tilde{\mu}_\mathrm{f}$ is the effective viscosity, k_f and k_s are the thermal conductivity of fluid and solid phases, respectively, and ρ_0 is the reference density.

The bounding horizontal surfaces of the porous layer are isothermal and impermeable. The appropriate boundary conditions on velocity and temperature are:

$$\mathbf{q} = 0,\ T_\mathrm{f} = T_\mathrm{s} = T_\mathrm{l} \text{ at } z = 0,$$
$$\mathbf{q} = 0,\ T_\mathrm{f} = T_\mathrm{s} = T_\mathrm{u} \text{ at } z = d.$$

The quantities are rendered to dimensionless form using the following transformations:

$$(x, y, z) = d(x^*, y^*, z^*),\quad \mathbf{q} = \frac{\varepsilon k_\mathrm{f}}{d(\rho c)_\mathrm{f}}\mathbf{q}^*,\quad t = \frac{(\rho c)_\mathrm{f} d^2}{k_\mathrm{f}}t^*,\quad p = \frac{\varepsilon \mu k_\mathrm{f}}{(\rho c)_\mathrm{f}}p^*,$$
$$\kappa_\mathrm{f} = \frac{k_\mathrm{f}}{(\rho c)_\mathrm{f}},\quad T_\mathrm{f} = (T_\mathrm{l} - T_\mathrm{u})\theta + T_\mathrm{u},\quad T_\mathrm{s} = (T_\mathrm{l} - T_\mathrm{u})\phi + T_\mathrm{u},\quad \nabla = \frac{\nabla^*}{d}. \tag{6}$$

Equations (1)–(5), using Eq. (6), become (after neglecting asterisks)

$$\nabla \cdot \mathbf{q} = 0, \tag{7}$$

$$\left(1 + \Lambda_1 \frac{\partial}{\partial t}\right)\left(-R_D \theta \hat{\mathbf{k}} + \nabla p\right) = -\left(1 + \Lambda_2 \frac{\partial}{\partial t}\right)\mathbf{q}, \tag{8}$$

$$\frac{\partial \theta}{\partial t} + (\mathbf{q}.\nabla)\theta = \nabla^2 \theta + H(\phi - \theta), \tag{9}$$

$$\alpha \frac{\partial \phi}{\partial t} = \nabla^2 \phi + \gamma H(\theta - \phi), \tag{10}$$

where

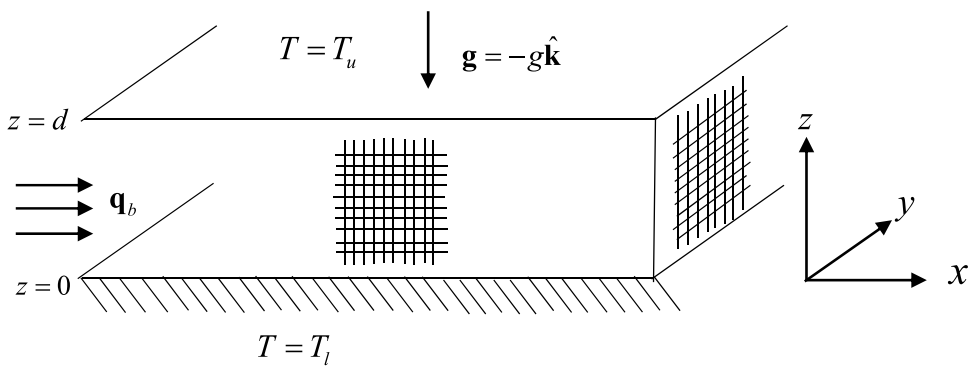

Fig. 1 Schematic representation of physical configuration

$$R_D = \frac{\rho_0 g\beta\Delta TKd(\rho c)_f}{\varepsilon\mu_f k_f}, H = \frac{hd^2}{\varepsilon k_f},$$
$$\alpha = \frac{k_f(\rho c)_s}{k_s(\rho c)_f} = \frac{\kappa_f}{\kappa_s}, \gamma = \frac{\varepsilon k_f}{(1-\varepsilon)k_s},$$
$$\Lambda_1 = \frac{\lambda_1 k_f}{(\rho c)_f d^2}, \Lambda_2 = \frac{\lambda_2 k_f}{(\rho c)_f d^2}.$$

are the Darcy–Rayleigh Number, scaled interphase heat transfer coefficient, ratio of diffusivities, ratio of porosity-modified conductivities, relaxation and retardation viscoelastic parameters, respectively.

The boundary conditions become

$$\mathbf{q} = 0 \text{ at } z = 0,\ 1,\ \ \theta = \phi = 1 \text{ at } z = 0,\ \theta = \phi = 0 \text{ at } z = 1. \tag{11}$$

3 Linear instability analysis

The basic state is characterized by

$$\mathbf{q}_b = u_b\,\hat{\mathbf{i}} = \Pi\,\hat{\mathbf{i}}, \theta_b = \phi_b = 1 - z, \tag{12}$$

where Π is the dimensionless constant horizontal pressure gradient and $\hat{\mathbf{i}}$ is the unit vector in the horizontal x-direction. The basic state is perturbed in the form

$$\mathbf{q} = \Pi\,\hat{\mathbf{i}} + \mathbf{q}',\ \ \theta = 1 - z + \theta',\ \ \phi = 1 - z + \phi', \tag{13}$$

where $\mathbf{q}'$, θ' and ϕ' are the perturbed quantities and assumed to be small. Equation (13) is substituted back in Eqs. (7)–(10), linearized, curl is operated on the momentum equation to discard the pressure term and the stream functions $\psi'(x,z,t)$ are introduced through

$$(u',\ 0,\ w') = \left(-\frac{\partial\psi'}{\partial z},\ 0,\ \frac{\partial\psi'}{\partial x}\right), \tag{14}$$

to obtain finally the stability equations in the form (after ignoring the primes)

$$\left(1 + \Lambda_2\frac{\partial}{\partial t}\right)\left(\nabla^2\psi\right) = R_D\left(1 + \Lambda_1\frac{\partial}{\partial t}\right)\frac{\partial\theta}{\partial x}, \tag{15}$$

$$\frac{\partial\theta}{\partial t} + \Pi\frac{\partial\theta}{\partial x} - \frac{\partial\psi}{\partial x} = \nabla^2\theta + H(\phi - \theta), \tag{16}$$

$$\alpha\frac{\partial\phi}{\partial t} = \nabla^2\theta + \gamma H(\theta - \phi). \tag{17}$$

The boundary conditions become

$$\psi = \ \theta = \phi = 0 \ \text{ at } \ z = 0, 1. \tag{18}$$

The normal mode analysis is employed in the form

$$(\psi, \theta, \phi) = [\Psi(z), \Theta(z), \Phi(z)]\exp\{ia(x - \omega t\}. \tag{19}$$

where $\omega(= \omega_r + i\omega_i)$ is the growth term and a is the horizontal wave number. Equation (19) is substituted back in Eqs. (15)–(18) to obtain, respectively,

$$\left(1 - ia\omega\Lambda_2\right)\left(D^2 - a^2\right)\Psi = iaR_D\left(1 - ia\omega\Lambda_1\right)\Theta, \tag{20}$$

$$ia\Psi + [(D^2 - a^2) - H + ia\omega - ia\Pi]\Theta + H\Phi = 0, \tag{21}$$

$$\gamma H\,\Theta + [(D^2 - a^2) - \gamma H + ia\omega\alpha]\Phi = 0. \tag{22}$$

where $D = \mathrm{d}/\mathrm{d}z$.

The associated boundary conditions are

$$\Psi = \ \Theta = \Phi = 0 \ \text{ at } \ z = 0, 1. \tag{23}$$

4 Numerical solution of the eigenvalue problem

Equations (20)–(23) form a complex stability eigenvalue problem and solved numerically to extract the critical eigenvalue R_{Dc} with respect to the wave number a as a function of Π, α, H, Λ_1, Λ_2 and γ. The Galerkin technique is utilized to solve the ensued stability eigenvalue problem, and accordingly $\Psi(z)$, $\Theta(z)$ and $\Phi(z)$ are expanded as follows [23]:

$$\Psi = \sum_{i=1}^{N} A_i\,\Psi_i(z),\ \ \Theta = \sum_{i=1}^{N} B_i\,\Theta_i(z),\ \ \Phi = \sum_{i=1}^{N} C_i\,\Phi_i(z). \tag{24}$$

Substituting Eq. (24) in Eqs. (20), (21) and (22) and multiplying the resulting equations by $\Psi_j(z)$,$\Theta_j(z)$ and $\Phi_j(z)$, respectively, and integrating with respect to z between $z = 0$ and 1, we get the following system of algebraic equations

$$L_{ji}A_i + M_{ji}B_i = \omega\{N_{ji}A_i + O_{ji}B_i\}, \tag{25}$$

$$P_{ji}A_i + Q_{ji}B_i + R_{ji}C_i = \omega S_{ji}B_i, \tag{26}$$

$$T_{ji}B_i + U_{ji}C_i = \omega V_{ji}C_i. \tag{27}$$

The coefficients $L_{ji} - V_{ji}$ involve inner products of the base functions and are given by

$$\begin{aligned}
&L_{ji} = a^2\langle \Psi_j\Psi_i\rangle + \langle D\Psi_j D\Psi_i\rangle,\ \ M_{ji} = iaR_D\langle \Psi_j\Theta_i\rangle,\\
&N_{ji} = ia\Lambda_2\{a^2\langle \Psi_j\Psi_i\rangle + \langle D\Psi_j D\Psi_i\rangle\},\\
&O_{ji} = ia\Lambda_1 R_D\langle \Psi_j\Theta_i\rangle,\ \ P_{ji} = -ia\langle \Theta_j\Psi_i\rangle,\\
&Q_{ji} = (a^2 + H + ia\Pi)\langle \Theta_j\Theta_i\rangle + \langle D\Theta_j D\Theta_i\rangle,\\
&R_{ji} = -H\langle \Theta_j\Phi_i\rangle,\ \ S_{ji} = ia\langle \Theta_j\Theta_i\rangle,\ \ T_{ji} = -H\gamma\langle \Phi_j\Theta_i\rangle,\\
&U_{ji} = (a^2 + H\gamma)\langle \Phi_j\Phi_i\rangle + \langle D\Phi_j D\Phi_i\rangle,\ \ V_{ji} = ia\alpha\langle \Phi_j\Phi_i\rangle,
\end{aligned} \tag{28}$$

where $\langle\cdots\rangle = \int_0^1 (\cdots)\,dz$. Equations (25)–(27) can be written in the matrix form

$$MX = \omega NX \tag{29}$$

where

$$M = \begin{bmatrix} L_{ji} & M_{ji} & 0 \\ P_{ji} & Q_{ji} & R_{ji} \\ 0 & T_{ji} & U_{ji} \end{bmatrix},\ N = \begin{bmatrix} N_{ji} & O_{ji} & 0 \\ 0 & S_{ji} & 0 \\ 0 & 0 & V_{ji} \end{bmatrix} \text{ and } X = \begin{bmatrix} A_i \\ B_i \\ C_i \end{bmatrix}.$$

We observe that M and N are complex matrices of order $3N \times 3N$, X is the characteristic vector and ω is the eigenvalue. By using the subroutine GVLRG of the ISML library, the complex eigenvalue problem ω is determined when the other parameters are specified. Then, one of the parameters, say R_D, is varied until the real part of $\omega\,(=\omega_r)$ vanishes. The zero crossing of ω_r is achieved by Newton's method for a fixed-point determination, and the imaginary part of $\omega\ (=\omega_i)$ indicates whether the instability onsets into steady convection ($\omega_i = 0$) or into growing oscillations ($\omega_i \neq 0$). The corresponding values of R_D and a are the critical conditions for neutral stability. Then, the critical Darcy–Rayleigh number with respect to the wave number is calculated using golden section search method. The base functions $\Psi_i(z)$, $\Theta_i(z)$ and $\Phi_i(z)$ are chosen such that they satisfy the respective boundary conditions

$$\Psi_i = z^i - z^{i+1} = \Theta_i = \Phi_i. \tag{30}$$

Equation (29) is a generalized eigenvalue problem and numerically solved following the procedure explained in the work of Shivakumara et al. [24].

5 Results and discussion

The impact of constant horizontal pressure gradient on the criterion for the onset of thermal convection in an Oldroyd-B fluid-saturated porous layer with LTNE temperatures is investigated. The critical Darcy–Rayleigh number R_{Dc}, the corresponding critical wave number a_c and the critical frequency of oscillations ω_{ic} are computed numerically, and the convergence is achieved by considering six terms in the Galerkin expansion. The progress of convergence is shown in Table 1 for various values of governing parameters. From the table, it is evident that there is not much deviation in the critical values between the first and higher order Galerkin methods. Hence, it is intuitive to look at the analytical solution for a single-term Galerkin method as it gives satisfactory results with minimum mathematical computations. Taking $N=1$ with sin πz as the trial function,

Table 1 Comparison of critical stability parameters calculated from single-term and different higher order Galerkin methods

N	$\Lambda_1 = 0.5,\ \Lambda_2 = 0.2$			$\Lambda_1 = 0.5,\ \Lambda_2 = 0.2$		
	$H = 10,\ \Pi = 0.1,\ \gamma = 1,\ \alpha = 0.5$			$H = 10,\ \Pi = 10,\ \gamma = 1,\ \alpha = 0.5$		
	a_c	R_{Dc}	ω_{ic}	a_c	R_{Dc}	ω_{ic}
1	3.75132	24.7666	2.4352	3.56195	21.9573	10.3234
2	3.88985	25.9414	2.4312	3.68705	23.1012	10.3425
3	3.73214	24.4594	2.4315	3.54130	21.6553	10.3174
4	3.73214	24.5312	2.4336	3.54467	21.7299	10.3189
5	3.73214	24.5354	2.4338	3.54486	21.7339	10.3190
6	3.73214	24.5354	2.4338	3.54485	21.7339	10.3190
Single-term	3.73123	24.5363	2.4339	3.54129	21.7329	10.3192

an analytical expression for R_D is obtained from Eq. (30) in the form

$$R_D = \frac{\delta^2}{a^2}\left[\frac{(1-ia\omega_i\Lambda_2)[(\delta^2+H+ia(\Pi-\omega))(\delta^2+H\gamma-\alpha ia\omega_i)-H^2\gamma]}{(H\gamma+\delta^2-\alpha ia\omega_i)(1-ia\omega_i\Lambda_1)}\right] \tag{31}$$

where $\delta^2 = a^2+\pi^2$. After removing the complex quantities from the denominator of Eq. (31), we obtain

$$R_D = \frac{1}{a^2\{k_8^2+a^2\alpha^2\omega_i^2\}(1+a^2\Lambda_1^2\omega_i^2)}\left[\Delta_1+i\omega_i\Delta_2\right] \tag{32}$$

where

$$\begin{aligned}\Delta_1 = {} & \delta^2[(\delta^2+a^2\alpha^2\omega_i^2)(-a^2(\Lambda_1-\Lambda_2)(\Pi-\omega_i)\omega_i+\delta^2(1+a^2\Lambda_1\Lambda_2\omega_i^2))+H^2\gamma(a^2(\Lambda_1-\Lambda_2)\omega_i(-\gamma\Pi+(\alpha+\gamma)\omega_i)\\ & +(1+\gamma)\delta^2(1+a^2\Lambda_1\Lambda_2\omega_i^2))+H(-2a^2\delta^2\gamma(\Lambda_1-\Lambda_2)(\Pi-\omega_i)\omega_i+(1+2\gamma)\delta^4(1+a^2\Lambda_1\Lambda_2\omega_i^2)+a^2\alpha_2\omega_i^2(1+a^2\Lambda_1\Lambda_2\omega_i^2))]\end{aligned} \tag{33}$$

$$\begin{aligned}\Delta_2 = {} & a\delta^2[H^2\gamma(\gamma\Pi-(k_{10}+\gamma k_{11})\omega_i+a^2\gamma\Lambda_1\Lambda_2\Pi\omega_i^2-a^2(\alpha+\gamma)\Lambda_1\Lambda_2\omega_i^3)+(\delta^4+a^2\alpha^2\omega_i^2)(\Pi(1+a^2\Lambda_1\Lambda_2\omega_i^2)\\ & -\omega_i(k_{11}+a^2\Lambda_1\Lambda_2\omega_i^2))+H((\Lambda_1-\Lambda_2)\omega_i(\delta^2+a^2\alpha^2\omega_i^2)+2\gamma\delta^2(\Pi(1+a^2\Lambda_1\Lambda_2)\omega_i^2-\omega_i(k_{11}+a^2\Lambda_1\Lambda_2\omega_i^2)))].\end{aligned} \tag{34}$$

The condition $\Delta_2 = 0$ gives a dispersion relation of the form

$$k_1\omega_i^5+k_2\omega_i^4+k_3\omega_i^3+k_4\omega_i^2+k_5\omega_i+k_6 = 0 \tag{35}$$

where

$$\begin{aligned}&k_1 = -\alpha^2a^2\Lambda_1\Lambda_2,\ k_2 = -\Pi k_1,\\ &k_3 = \delta^2[\alpha^2k_7-(H^2\alpha\gamma\Lambda_1\Lambda_2+k_8^2\Lambda_1\Lambda_2)],\\ &k_4 = a^2(\alpha^2+k_8^2\Lambda_1\Lambda_2)\Pi,\\ &k_5 = a^2[k_9+H(2\gamma\delta^2k_9++\delta^4(\Lambda_1-\Lambda_2))-H^2\gamma(k_{10}+\gamma k_{11})],\\ &k_6 = k_8^2\Pi,\ k_7 = [-1+(H+\delta^2)(\Lambda_1-\Lambda_2)],\\ &k_8 = (H\gamma+\delta^2),\ k_9 = [-1+\delta^2(\Lambda_1-\Lambda_2)],\\ &k_{10} = [\alpha+\delta^2(-\Lambda_1+\Lambda_2)],\\ &k_{11} = [1+\delta^2(-\Lambda_1+\Lambda_2)].\end{aligned} \tag{36}$$

The critical values of R_D and ω_i over a are computed numerically, and the values are given in the end of Table 1, and it is seen that there is an excellent agreement between the results obtained from single-term and higher order Galerkin methods. The results obtained under the limiting case of $\Lambda_1 = \Lambda_2 = 0$(Newtonian fluid) by taking six terms in the Galerkin expansion are compared with those of Postelnicu [22] obtained using the numerical solver *dsolve* from Maple in Table 2. We note that the results obtained from two different methods are in close agreement indicating the validity of numerical method employed.

Table 2 Comparison of critical stability parameters for different values of governing parameters

	Postelnicu [22]		Present study	
	a_c	R_{Dc}	a_c	R_{Dc}
$\Pi = 0.1$, $H = 10$, $\gamma = 1$	3.436	52.360	3.4363	52.3598
$\Pi = 1$, $H = 1$, $\gamma = 1$	3.211	41.363	3.2114	41.3626
$\Pi = 10$, $H = 10$, $\gamma = 1$	3.529	54.387	3.4876	53.589
$\Pi = 10$, $H = 1000$, $\gamma = 1$	3.148	78.617	3.1526	78.4039
$\Pi = 10$, $H = 1000$, $\gamma = 10$	3.142	43.427	3.1417	43.4229
$\Pi = 100$, $H = 100$, $\gamma = 0.01$	5.730	185.54	5.7370	185.531

The viscoelastic parameters influence only the oscillatory onset and not the stationary convection. This is because viscoelastic fluid of simple type becomes Newtonian when the flow is steady and weak and hence the viscoelasticity produces nothing new on the onset of stationary convection. Thus, there is no distinction between viscous fluid and viscoelastic fluid as far as the stationary convection is concerned. However, in the case of oscillatory convection (time-dependent motion), the viscoelastic relaxation and retardation time parameters influence the oscillatory onset. The neutral stability curves in the (R_D, a)-plane for various values of Λ_1, Λ_2, γ, Π, H and α are displayed in Fig. 2a–f. It is noted that the neutral curves are unimodal and akin to those seen in the classical Darcy–Bénard problem. In addition, Λ_1 and Λ_2 have contradictory influences on the instability characteristics of the system. In particular, increase in Λ_1 (Fig. 2a) and Λ_2 (Fig. 2b) is to increase and decrease the instability region, respectively. The neutral curve shown for $\Lambda_2 = 0$ in Fig. 2b corresponds to that for a Maxwell fluid. Furthermore, increase in γ (Fig. 2c) and Π (Fig. 2d) is to increase the instability region, whereas an opposite behavior is noticed for decreasing H (Fig. 2e) and α (Fig. 2f). Besides, the oscillatory neutral stability curves tilt toward lower values of the wave number when the values of Λ_1, γ and Π increase. This amounts to a reduction in the critical wave number indicating an increase in the cell width.

Figure 3a–c demonstrates the way in which R_{Dc}, a_c and ω_{ic} vary with Π for different values of H when $\alpha = 0.5$, $\Lambda_1 = 0.5$ and $\Lambda_2 = 0.2$. Figure 3a suggests that R_{Dc} is inversely proportional to Π and it remains invariant with increasing Π. It is noted that an increase in H is to increase R_{Dc} due to an increase in rapid heat exchange between the fluid and solid phases of the porous medium and also

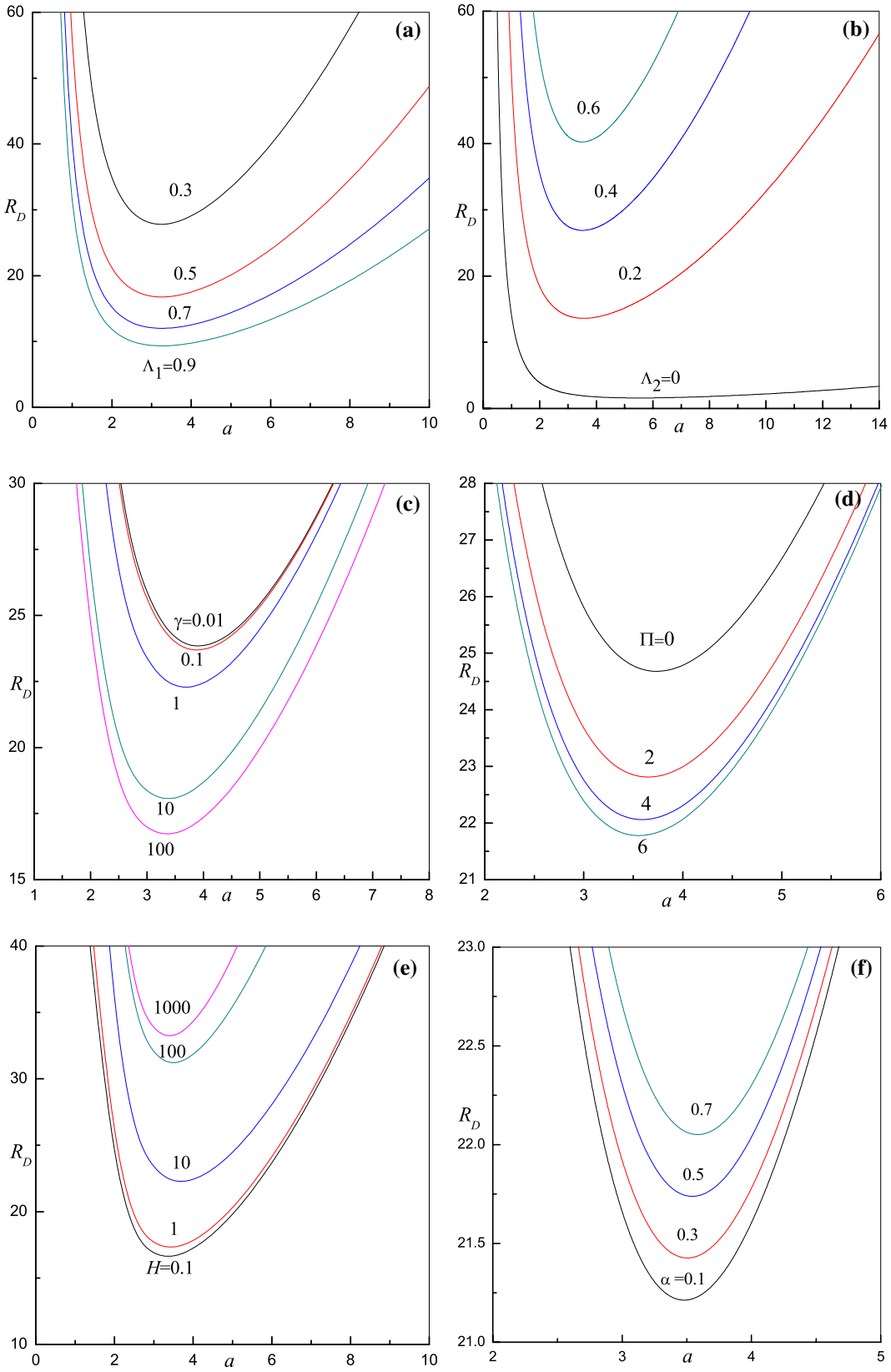

Fig. 2 Neutral stability curves for different values of **a** Λ_1 with $\Lambda_2 = 0.2$, **b** Λ_2 with $\Lambda_1 = 1$ when $H = 10$, $\alpha = 0.5$, $\gamma = 1$ and $\Pi = 10$, **c** γ with $\Pi = 10$, **d** Π with $\gamma = 1$ when $H = 10$, $\alpha = 0.5$, $\Lambda_1 = 0.5$ and $\Lambda_2 = 0.2$, **e** H with $\alpha = 0.5$ and **f** α with $H = 10$ when $\Pi = 10$, $\gamma = 1$, $\Lambda_1 = 0.5$ and $\Lambda_2 = 0.2$

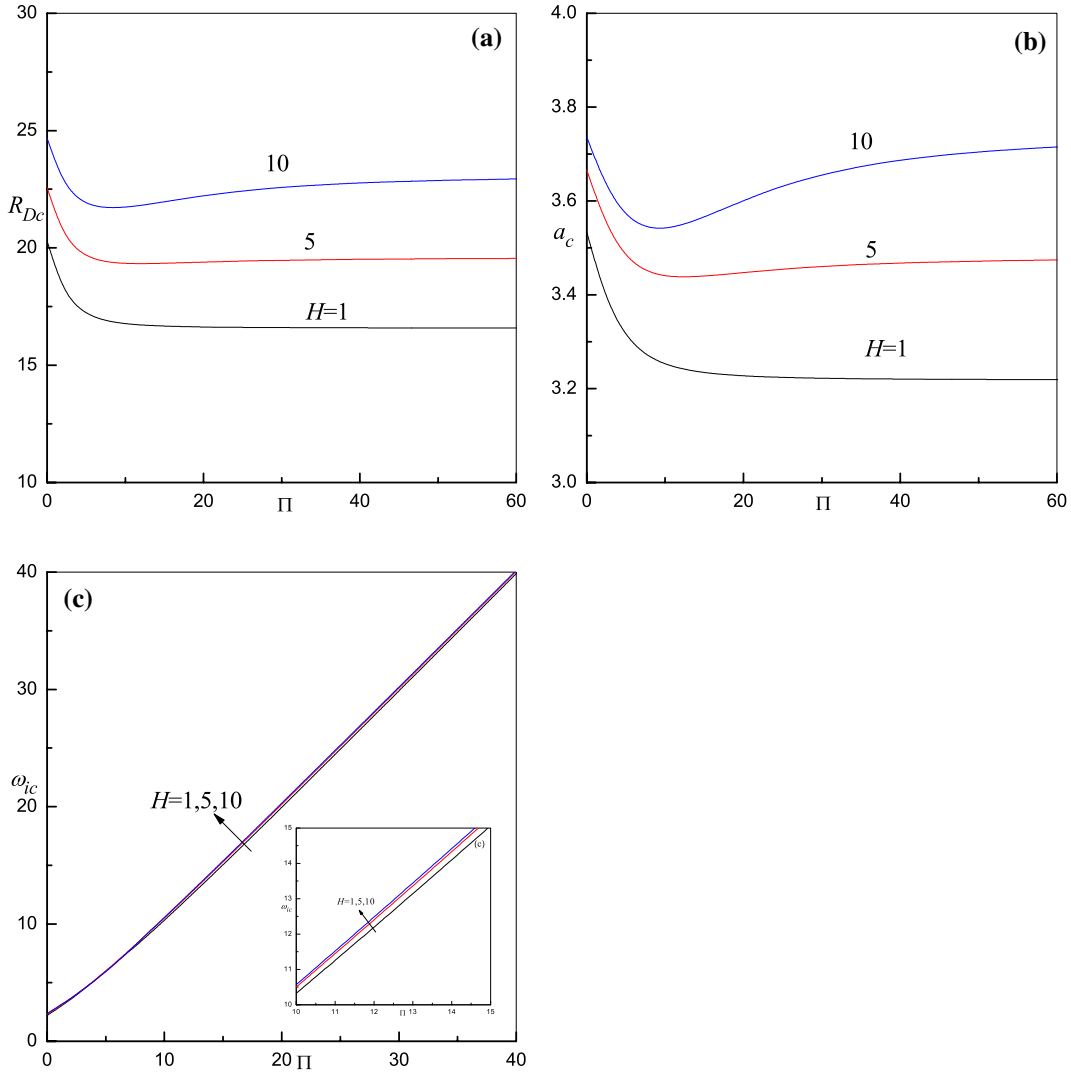

Fig. 3 Variation in **a** critical Darcy–Rayleigh number vs the pressure gradient Π, **b** critical wave number vs the pressure gradient Π and **c** critical frequency vs the pressure gradient Π, when $\alpha = 0.5, \gamma = 1, \Lambda_1 = 0.5$ and $\Lambda_2 = 0.2$

increase in residence of time of heat in solid phase. Hence, its effect is to delay the onset of convection. Figure 3b illustrates that a_c diminishes initially up to certain values of Π, but remains unchanged with increasing values of Π. Also note that increasing H is to increase a_c and as a result the size of the convection cell decreases. Figure 3c displays the variation in ω_{ic} as a function of Π, and note that all the curves increase gradually irrespective of values of H. The variation in R_{Dc}, a_c and ω_{ic} as a function of Π for different values of γ is shown in Fig. 4a–c. The influence of γ on the critical stability parameters with Π turns out to be opposite to that of H as observed in Fig. 3a–c.

The impact of viscoelastic parameters Λ_1 and Λ_2 on the critical values of R_{Dc}, a_c and ω_{ic} is illustrated in Fig. 5a–c as a function of Π when $\alpha = 0.5, H = 10$ and $\gamma = 1$. From Fig. 5a, it is clear that R_{Dc} passes through a minimum with increasing Π before attaining a constant value at higher values of Π. This trend is found to be the same for all the values of Λ_1 and Λ_2 considered. It is also noticed that increase in Λ_1 is to decrease R_{Dc} because of allowing the applied stress to act for a longer time on the fluid. In fact, the increase in relaxation ceases the stickiness of the fluid and hence the effect of friction will be lesser so that convection sets in at lower values of R_{Dc}. An opposite phenomenon is observed with increase in Λ_2. That is, increase in the value of Λ_2 is to delay the onset of convection because of increase in the retardation effect. Moreover, the curves of $\Lambda_2 \neq 0$ lie above the curve of $\Lambda_2 = 0$, which indicates that the stickiness of Maxwell fluid is less compared to an Oldroyd-B fluid. Figure 5b demonstrates that a_c decreases initially up to certain values of Π, but gradually increases for increasing values of Π. Eventually, all the curves of a_c

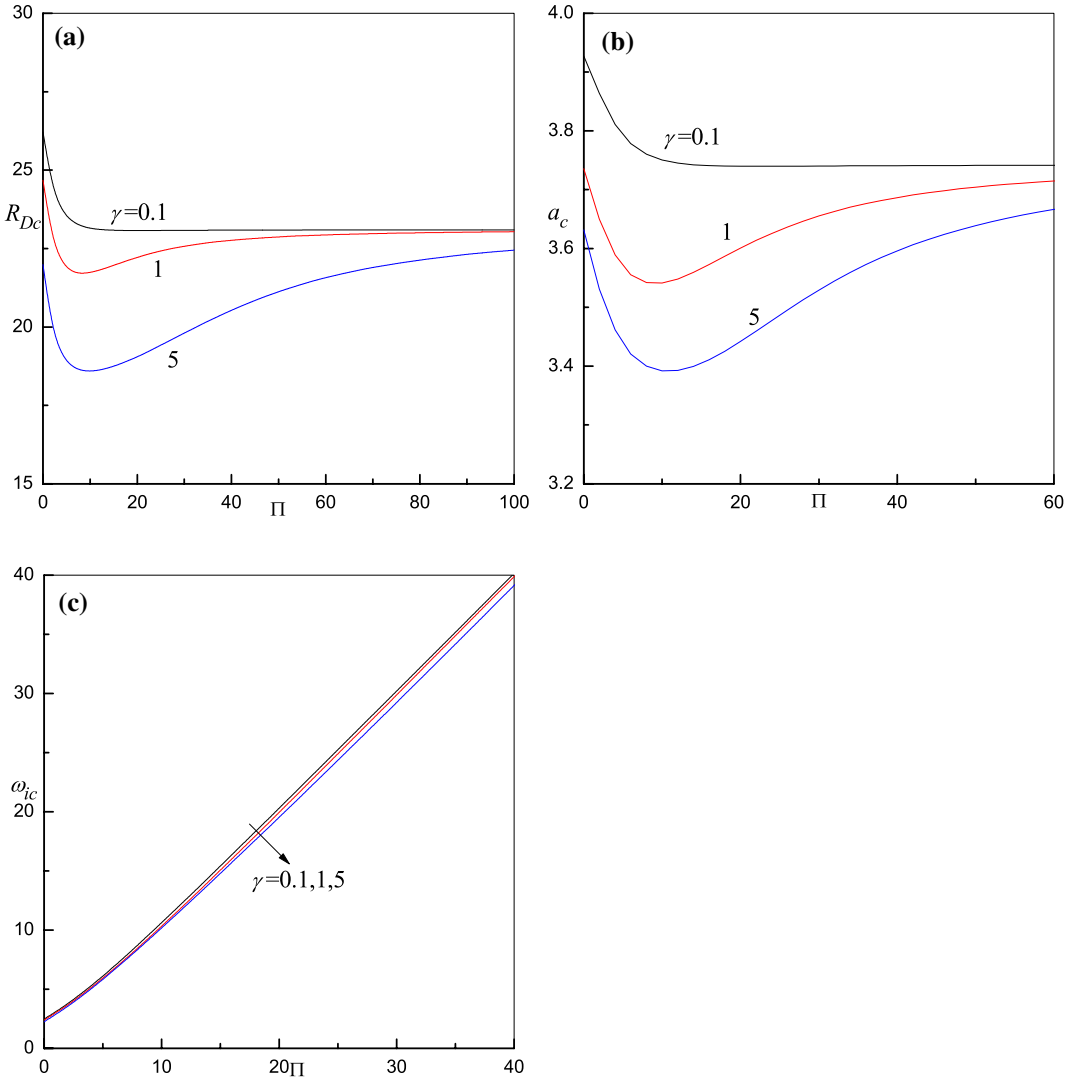

Fig. 4 Variation in **a** critical Darcy–Rayleigh number vs the pressure gradient Π, **b** critical wave number vs the pressure gradient Π and **c** critical frequency vs the pressure gradient Π, when $\alpha = 0.5$, $H = 10$, $\Lambda_1 = 0.5$ and $\Lambda_2 = 0.2$

for different Λ_1 and Λ_2 coalesce at higher values of Π. From Fig. 5c, we observe that an increase in Π is to increase ω_{ic} rapidly for various values of Λ_1 and Λ_2.

Figure 6a–c demonstrates the variation in R_{Dc}, a_c and ω_{ic} with Λ_2 for various values of Π and Λ_1 when $\alpha = 0.5$, $H = 10$ and $\gamma = 1$. Figure 6a shows that increase in Π and Λ_1 is to decrease the critical Darcy–Rayleigh number for a fixed value of Λ_2, and therefore its effect is to hasten the onset of oscillatory convection. On the contrary, increasing Λ_2 delays the onset of oscillatory convection. This is because increasing Λ_2 amounts to increase in time taken by the fluid element to respond to the applied stress. For a fixed values of Λ_1, there exists a threshold value of $\Lambda_2 = \Lambda_2^*$ beyond which the stationary convection prevails, and note that increase in Π is to increase Λ_2^*. From Fig. 6b, it is observed that the curves of a_c drop suddenly and remain invariant for different values of Π and Λ_1 at those values of Λ_2 at which the preferred mode of instability switches over from oscillatory to stationary convection. Also, increase in Π decreases a_c and hence increases the convection cells size, whereas an opposite trend could be seen with increasing Λ_1. The value of ω_{ic} decreases with increasing Λ_2 and increases with increasing Π and Λ_1 (Fig. 6c) due to an increase in the elasticity of the fluid.

The plots of R_{Dc}, a_c and ω_{ic} with $\log_{10}H$ are depicted in Fig. 7a–c for different values of Π when $\alpha = 0.5$, $\gamma = 1$, $\Lambda_1 = 0.5$ and $\Lambda_2 = 0.2$. From Fig. 7a, it is observed that R_{Dc} increases gradually with H, reaches a maximum and remains constant subsequently with further increase in H. Also, R_{Dc} decreases with increasing Π because increase in Π leads to prominent heat transfer through both the

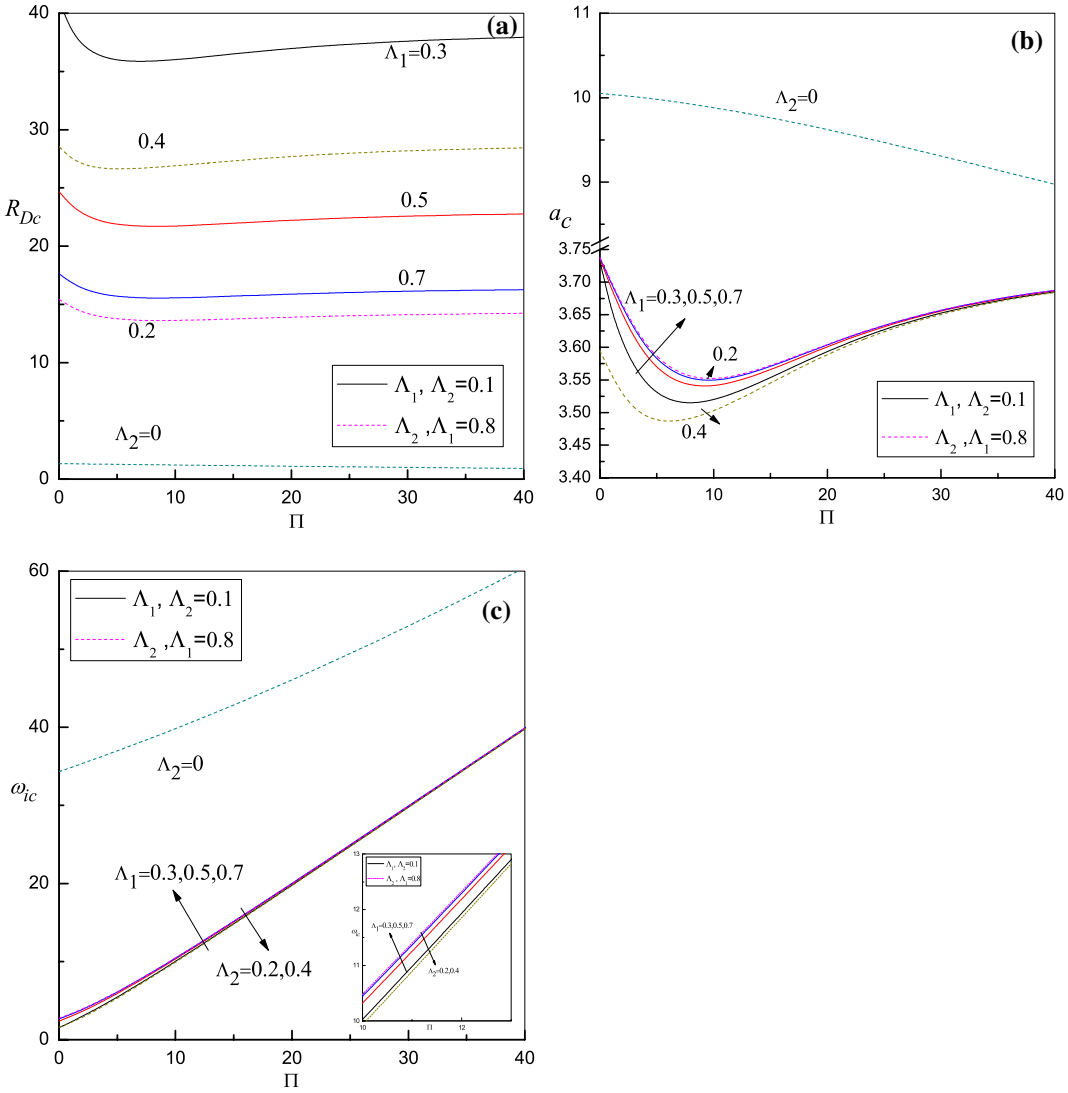

Fig. 5 **a** Critical Darcy–Rayleigh number vs the pressure gradient Π, **b** critical wave number vs the pressure gradient Π and **c** critical frequency vs the pressure gradient Π, when $\alpha = 0.5, H = 10$ and $\gamma = 1$

phases which in turn eases the stabilizing effect of H and speeds up the onset of oscillatory convection. Figure 7b indicates that a_c remains unaffected in the small-H and large-H limits, whereas at intermediate values of H it reaches maximum values for various values of Π. We note that a_c decreases with increasing Π at intermediate values of H and as a result the convection cells size increases. From Fig. 7c, increase in ω_{ic} is noted as Π increases.

To know distinctly the effect of individual and simultaneous presence of horizontal pressure gradient and the viscoelasticity of the fluid on the convective instability, the values of R_{Dc}, a_c and ω_{ic} computed for these cases are given in Table 3. It is observed that oscillatory convection is possible even in the isolation presence of pressure gradient and viscoelasticity: a result of contrast in which stationary convection is only possible in their absence. In the case of Newtonian fluids ($\Lambda_1 = 0 = \Lambda_2$), the effect of increasing Π is found to increase R_{Dc} marginally and hence to delay the onset of oscillatory convection, while R_{Dc} decreases slightly with increasing Π if the fluid is viscoelastic and hence to hasten the onset of oscillatory convection. Nevertheless, the frequency of oscillations increases with increasing Π irrespective of whether the fluid is Newtonian or viscoelastic.

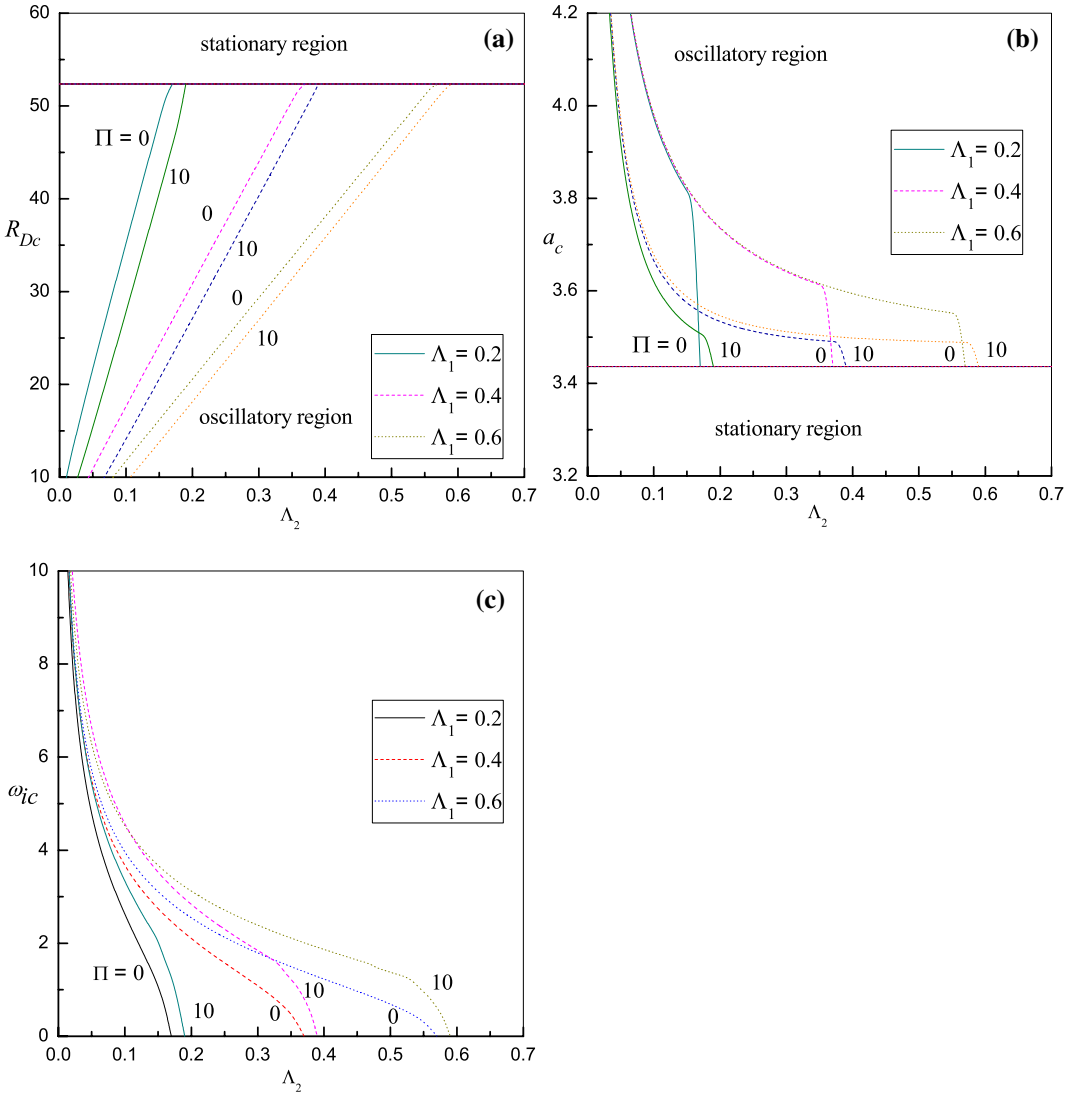

Fig. 6 Variation in **a** R_{Dc}, **b** a_c and **c** ω_{ic} with Λ_2 for different Π when $H = 10, \gamma = 1$ and $\alpha = 0.5$

6 Conclusions

The implications of a constant horizontal pressure gradient and LTNE temperatures on the onset of thermal convective instability of an Oldroyd-B fluid-saturated porous medium are explored. The stability eigenvalue problem with complex coefficients is solved numerically.

The important findings of the present study may be summarized as follows:

1. Contrary to the observed phenomenon in Newtonian fluids, the effect of constant horizontal pressure gradient Π is to hasten the onset of oscillatory convection in an Oldroyd-B fluid-saturated porous layer.
2. The extent to which the relaxation (Λ_1) and the retardation (Λ_2) viscoelastic parameters encompass opposite contributions on the onset of oscillatory convection is to diminish in the presence of pressure gradient. The impact of increasing Λ_1 is to advance marginally while increasing Λ_2 is to suppress noticeably the onset of oscillatory convection.
3. The range of values of retardation parameter Λ_2 up to which the instability sets in as oscillatory convection increases with increasing Π.

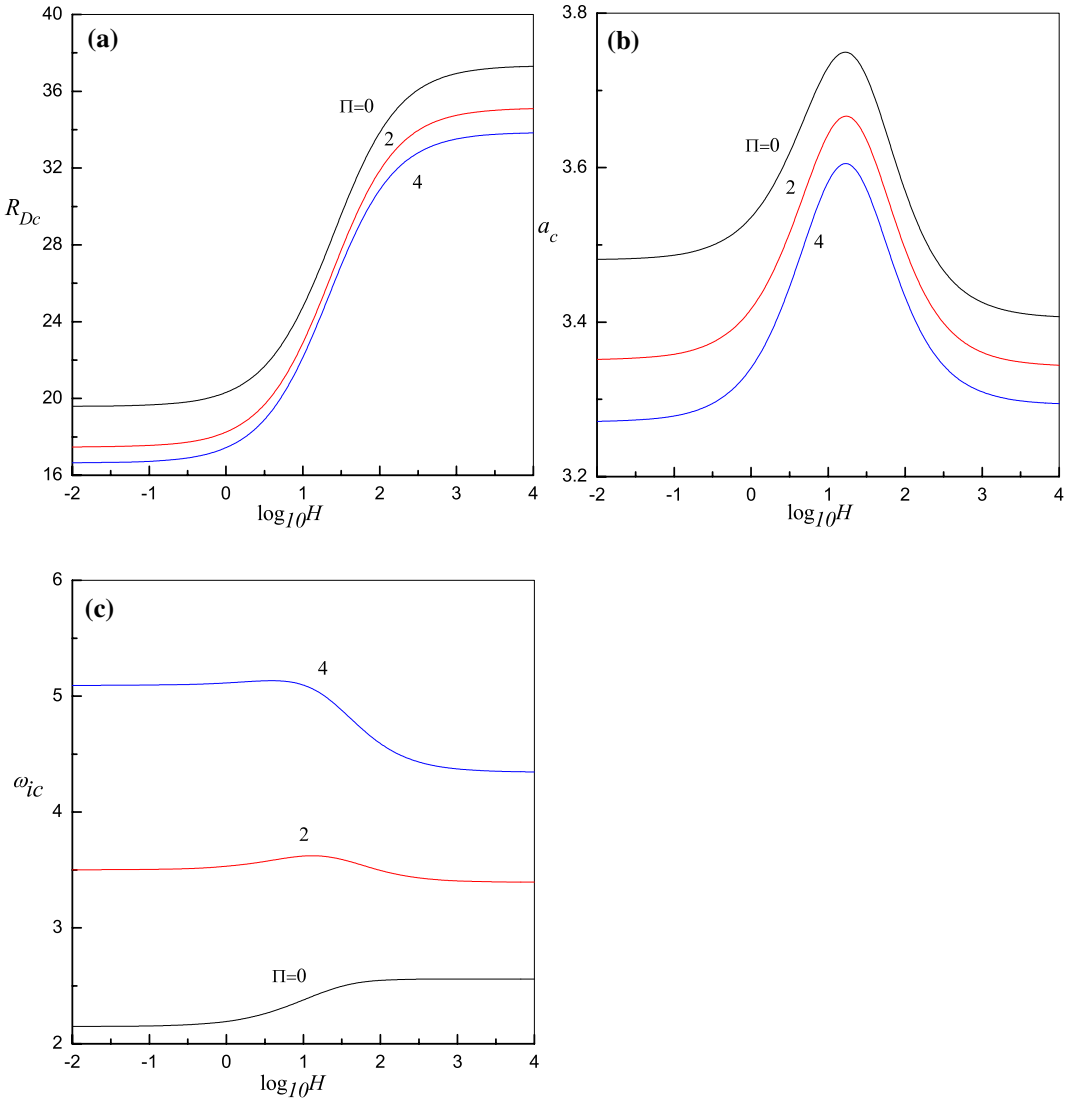

Fig. 7 Variation in **a** R_{Dc}, **b** a_c and **c** ω_{ic} with $\log_{10}H$ for different Π when $\alpha = 0.5$, $\Lambda_1 = 0.5$, $\gamma = 1$ and $\Lambda_2 = 0.2$

4. Increasing Π is to increase the convection cells size of oscillatory onset and also the critical frequency of oscillations.
5. Both large and small values of interphase heat transfer coefficient H have no noticeable impact on the oscillatory onset but the intermediate values of H exhibit strong influence on the onset of oscillatory convection.
6. The system is more unstable for Maxwell fluid than that of Oldroyd-B type of viscoelastic fluid.

Table 3 Critical values for different values of pressure gradient and viscoelastic parameters

Case	Π	Λ_1	Λ_2	R_{Dc}	a_c	ω_{ic}
I	2	0	0	52.4209	3.43854	1.90612
	5			52.7234	3.44992	4.77824
	10			53.5897	3.48761	9.63187
II	0	0.8	0.2	15.4284	3.73786	2.74232
			0.4	28.5559	3.59508	1.58436
			0.6	41.652	3.5434	0.87401
III	0	0.3	0.1	23.4713	3.97683	3.35937
		0.5		14.0907	3.97979	3.84943
		0.7		10.0672	3.98103	4.04132
IV	2	0.5	0.2	22.8064	3.64975	3.623
	5			21.8762	3.56917	5.91084
	10			21.733	3.54129	10.3192
V	10	0.8	0.2	13.6232	3.55209	10.4781
			0.4	26.8939	3.50298	9.93235
			0.6	40.2316	3.49182	9.73422
VI	10	0.3	0.1	18.7082	3.65058	11.0136
		0.5		11.3028	3.67271	11.2587
		0.7		8.09605	3.6815	11.3612

Acknowledgements One of the authors CH is grateful to the SC/ST cell of Bangalore University, Bengaluru, for granting him a scholarship to carry out his research work. The authors wish to thank the reviewers for their constructive comments which helped in improving the paper considerably.

Compliance with ethical standards

Conflict of interest On behalf of authors, the corresponding author states that there is no conflict of interest.

References

1. Carbonell RG, Whitaker S (1984) Heat and mass transport in porous media. In: Bear J, Corapcioglu MY (eds) Fundamentals of transport phenomena in porous media. Springer, Dordrecht, pp 121–198
2. Rees DAS (2010) Microscopic modelling of the two-temperature model for conduction in heterogeneous media. J Porous Med 13(2):125–143
3. Straughan B (2015) Convection with local thermal non-equilibrium and micro fluidic effects. Springer, Heidelberg
4. Virto L, Carbonell M, Castilla R, Gamez-Montero PJ (2009) Heating of saturated porous media in practice: several causes of local thermal non-equilibrium. Int J Heat Mass Transf 52:5412–5422
5. Banu N, Rees DAS (2002) Onset of Darcy-Benard convection using a thermal non- equilibrium model. Int J Heat Mass Transf 45:2221–2228
6. Postelnicu A, Rees DAS (2003) The onset of Darcy-Brinkman convection in a porous layer using a thermal non-equilibrium model. Part I: stress-free boundaries. Int J Energy Res 27:961–973
7. Malashetty MS, Shivakumara IS, Kulkarni S (2005) The onset of convection in an anisotropic porous layer using a thermal non-equilibrium model. Transp Porous Med 60:199–215
8. Malashetty MS, Shivakumara IS, Kulkarni S (2005) The onset of Lapwood–Brinkman convection using a thermal non-equilibrium model. Int J Heat Mass Transf 48:1155–1163
9. Malashetty MS, Swamy M, Kulkarni S (2007) Thermal convection in a rotating porous layer using local thermal non-equilibrium model. Phys Fluids 19:054102
10. Shivakumara IS, Mamatha AL, Ravisha M (2010) Boundary and thermal nonequilibrium effects on the onset of Darcy-Brinkman convection in a porous layer. J Eng Math 67:317–328
11. Lagziri H, Barletta A, Celli M, Bezzazi, M (2016) The onset of Darcy–Bénard instability in a horizontal porous channel with a free surface using a thermal non-equilibrium model. In: MATEC Web of Conferences vol 83, p 07003
12. Celli M, Lagziri H, Bezzazi M (2017) Local thermal non-equilibrium effects in the Horton–Rogers–Lapwood problem with a free surface. Int J Therm Sci 116:254–264
13. Lagziri H, Bezzazi M (2019) Robin boundary effects in the Darcy–Bénard problem with LTNE model. Transp Porous Med 129:701–720
14. Rees DAS, Pop I (2005) Local thermal non-equilibrium in porous medium convection. In: Transport phenomena in porous media III. Pergamon, pp 147–175
15. Neild DA, Bejan A (2017) Convection in porous media, 5th edn. Springer, New York
16. Malashetty MS, Shivakumara IS, Kulkarni S, Swamy M (2006) Convective instability of Oldroyd-B fluid saturated porous layer heated from below using a thermal non-equilibrium model. Trans Porous Med 64:123–139
17. Shivakumara IS, Malashetty MS, Chavaraddi KB (2006) Onset of convection in a viscoelastic fluid-saturated sparsely packed porous layer using a thermal non-equilibrium model. Can J Phys 84:973–990
18. Malashetty MS, Kulkarni S (2009) The convective instability of Maxwell fluid saturated porous layer using a thermal non-equilibrium model. J Non Newton Fluid 16(1–3):29–37

19. Shankar BM, Shivakumara IS (2017) Effect of local thermal nonequilibrium on the stability of natural convection in an oldroyd-B fluid saturated porous layer. ASME 139:044503-1
20. Prats M (1967) The effect of horizontal fluid motion on thermally induced convection currents in porous medium. J Geophys Res 71:4835–4848
21. Postelincu A (2007) The effect of inertia on the onset of mixed convection in a porous layer using a thermal non-equilibrium model. J Porous Med 10:515–524
22. Postelincu A (2010) The effect of a horizontal pressure gradient on the onset of a Darcy-Benard convection in thermal non-equilibrium conditions. Int J Heat Mass Transf 53:68–75
23. Finlayson BA (1972) The method of weighted residuals and variational principles. Academic Press, New York
24. Shivakumara IS, Dhananjaya M, Ng Chiu-On (2015) Thermal convective instability in an Oldroyd-B nanofluid saturated porous layer. Int J Heat Mass Transf 84:167–177